How to cite: *Angew. Chem. Int. Ed.* **2022,** *61*, e202204953
International Edition: doi.org/10.1002/anie.202204953
German Edition: doi.org/10.1002/ange.202204953

Monolayer Photosensitizers

Two-Dimensional Photosensitizer Nanosheets via Low-Energy Electron Beam Induced Cross-Linking of Self-Assembled Ru^{II} Polypyridine Monolayers

*Maria Küllmer, Felix Herrmann-Westendorf, Patrick Endres, Stefan Götz, Hamid Reza Rasouli, Emad Najafidehaghani, Christof Neumann, Rebecka Gläßner, David Kaiser, Thomas Weimann, Andreas Winter, Ulrich S. Schubert, Benjamin Dietzek-Ivanšić, and Andrey Turchanin**

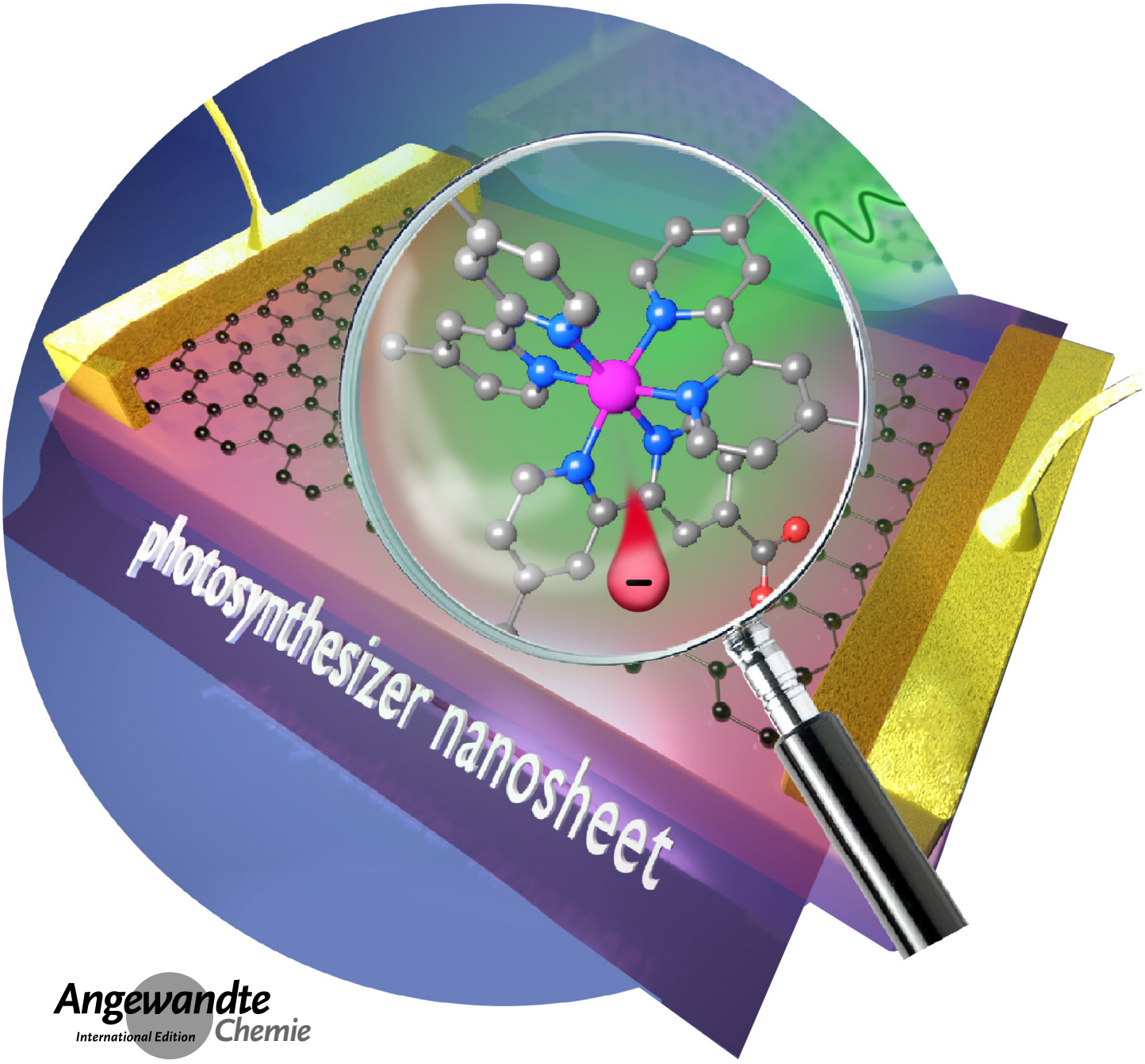

Abstract: Artificial photosynthesis for hydrogen production is an important element in the search for green energy sources. The incorporation of photoactive units into mechanically stable 2D materials paves the way toward the realization of ultrathin membranes as mimics for leaves. Here we present and compare two concepts to introduce a photoactive Ru^{II} polypyridine complex into ≈1 nm thick carbon nanomembranes (CNMs) generated by low-energy electron irradiation induced cross-linking of aromatic self-assembled monolayers. The photoactive units are either directly incorporated into the CNM scaffold or covalently grafted to its surface. We characterize Ru^{II} CNMs using X-ray photoelectron, surface-enhanced Raman, photothermal deflection spectroscopy, atomic force, scanning electron microscopy, and study their photoactivity in graphene field-effect devices. Therewith, we explore the applicability of low-energy electron irradiation of metal complexes for photosensitizer nanosheet formation.

The increasing demand for sustainable energy sources leads to the development of various artificial photocatalytic systems to replace fossil fuels with "green" hydrogen.[1] These synthetic leaves imitate the natural photosynthesis and act as catalysts for the conversion of water upon irradiation with visible light.[1b] In artificial photosynthesis, molecular photosensitizers, e.g., Ru^{II} polypyridine complexes,[2] are regularly employed as their photoactivity and charge-transfer properties can be tuned by adjusting the molecular structure.[1b,3] The incorporation of molecular photosensitizers into an ultrathin nanosheet is particular promising as in this case the single molecules function is combined with the structural integrity of a solid. This integration allows miniaturization of the photoactive device[3] and increases the photosensitizers recyclability and stability.[4] Furthermore, such material design can be expanded to asymmetrically functionalized membranes, in which an electron acceptor is linked to one side of the membrane, while an electron donor functionalizes the opposite surface. Two-dimensional (2D) materials like transition metal dichalcogenides, graphene, carbon nitrides or carbon nanomembranes (CNMs), as platforms for artificial leaves, provide exceptionally high surface/volume ratios which are crucial for catalytic efficiency.[5] Furthermore, 2D materials have the potential to serve simultaneously as separator membranes for reaction products due to their mechanical stability and tunable permeation for gases.[6] The photoactivity of 2D materials can be adjusted via doping with single atoms or introduction of single molecules.[3,5b,7] However, functionalization of 2D materials with photoactive units requires mostly a hierarchical step by step assembly which can result in defects in the 2D platform caused by harsh reaction conditions or suffer from low coupling efficiencies.[8] CNMs prepared by low-energy electron irradiation of self-assembled monolayers (SAMs) allow variation of their chemical and permeation properties as these characteristics strongly correlate with the employed molecular precursors.[9] Here, we demonstrate that molecular photosensitizer nanosheets with ≈1 nm thickness can be synthesized directly via the electron irradiation induced cross-linking of Ru^{II} polypyridine complex SAMs.

The general process of the nanosheet formation is shown in Figure 1. Experimental details are presented as well in Scheme 1 and the Supporting Information. First, a SAM of the complex **1** $[Ru(dmbpy)_2(dcbpy)](PF_6)_2$ (dmbpy: 4,4′-dimethyl-2,2′-bipyridine; dcbpy: 2,2′-bipyridine-4,4′-dicarboxylic acid) is formed by immersion of Au/mica substrates in a dimethylformamide (DMF) solution of complex **1**.[10] Formation of Ru^{II} SAM **2a** takes place upon deprotonation of the carboxyl groups and their attachment to the substrate; by adjusting temperature, the layer thickness can be tuned.[10] As we report next, irradiation of Ru^{II} SAM **2a** with low-energy electrons (electron energy 50 eV, dose 50 mC cm^{-2}) leads to the cross-linking between adjacent molecules, as shown for small linear aromatic molecules, e.g., 4′-nitro[1,1′-biphenyl]-4-thiol (**3**, NBPT)[11] and [1,1′-biphenyl]-4-thiol (BPT).[12] In this way a continuous and mechanically stable nanosheet is formed (Ru^{II} CNM **2b**) from the parent Ru^{II} polypyridine complexes. The nanosheet can be removed from the growth substrate via a polymer assisted transfer[13] and placed on different substrates, e.g., Si wafer, quartz or holey substrates. We study the formation of

[*] M. Küllmer, F. Herrmann-Westendorf, H. Reza Rasouli, E. Najafidehaghani, C. Neumann, R. Gläßner, D. Kaiser, B. Dietzek-Ivanšić, A. Turchanin
Institute of Physical Chemistry
Friedrich Schiller University Jena
07743 Jena (Germany)
E-mail: andrey.turchanin@uni-jena.de

F. Herrmann-Westendorf, B. Dietzek-Ivanšić
Leibniz Institute of Photonic Technology e. V. (IPHT), Research Department Functional Interfaces
07745 Jena (Germany)

P. Endres, S. Götz, A. Winter, U. S. Schubert
Laboratory of Organic and Macromolecular Chemistry (IOMC), Friedrich Schiller University Jena
07743 Jena (Germany)

T. Weimann
Physikalisch-Technische Bundesanstalt (PTB)
38116 Braunschweig (Germany)

U. S. Schubert, B. Dietzek-Ivanšić, A. Turchanin
Center for Energy and Environmental Chemistry Jena (CEEC Jena)
07743 Jena (Germany)

U. S. Schubert, B. Dietzek-Ivanšić, A. Turchanin
Jena Center for Soft Matter (JCSM)
Friedrich Schiller University Jena
07743 Jena (Germany)

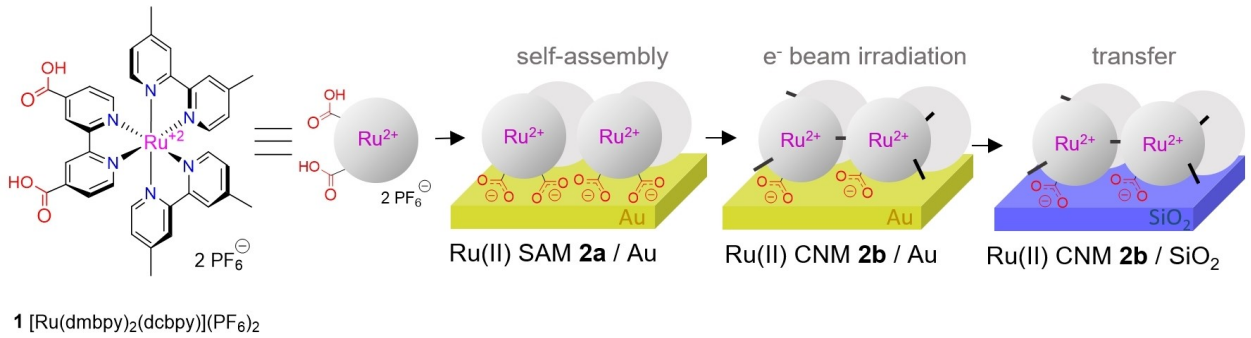

Figure 1. General preparation procedure of a photosensitizer nanosheet. Self-assembly of compound **1** on gold generates Ru^{II} SAM **2a**. Irradiation with low-energy electrons leads to cross-linking and formation of Ru^{II} CNM **2b**. The nanosheet **2b** can be transferred to various solid or holey target substrates, e.g., SiO_2/Si wafers or TEM grids.

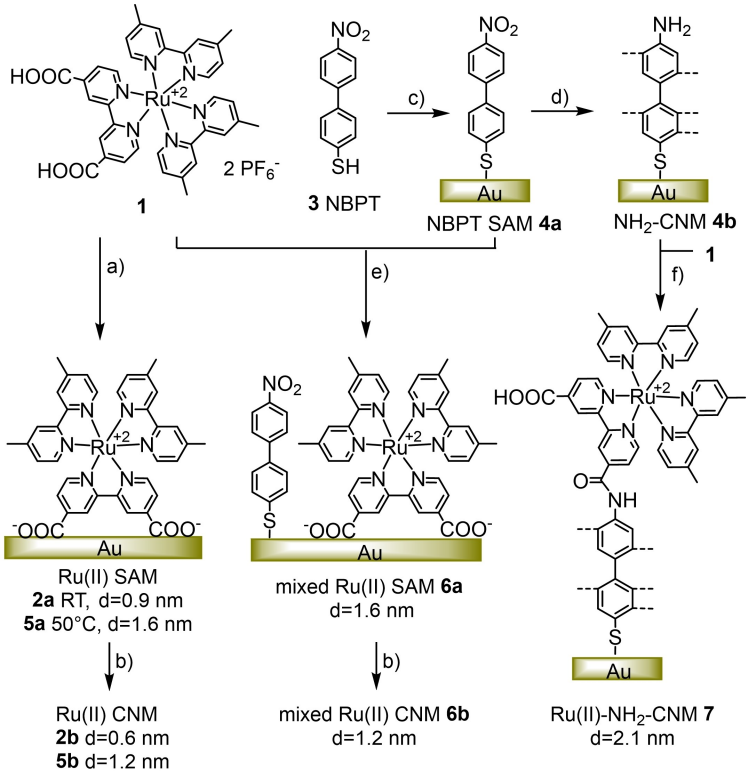

Scheme 1. Synthesis of different photosensitizer nanosheets. The layer thickness d on gold was obtained by X-ray photoelectron spectroscopy. Experimental conditions: a) **1** (0.07 mM), Au/mica, DMF, 72 h, RT or 50 °C; b) electron beam irradiation (50 eV, 50 mC cm^{-2}); c) Au/mica, **3** (0.22 mM), DMF d) electron beam irradiation (100 eV, 50 mC cm^{-2}); e) NBPT SAM **4a**, **1** (0.37 mM), DMF, 45 °C, 28 h; f) NH_2-CNM **4b**, **1** (0.013 mmol), PyBOP (0.026 mmol), DIPEA (0.054 mmol), DMF (30 mL), 70 °C, 4 h 30 min.

these molecular photosensitizer nanosheets, their physical, chemical and functional properties employing complementary microscopy and spectroscopy techniques including atomic force microscopy (AFM), optical microscopy, scanning electron microscopy (SEM), X-ray photoelectron spectroscopy (XPS), Raman scattering and photothermal deflection spectroscopy (PDS).

First, the formed nanosheets were studied by AFM, optical microscopy and SEM in order to investigate their structural integrity. The AFM images of Ru^{II} CNMs **2b**, generated from the monolayers self-assembled at room temperature (RT), are shown in Figures 2a and b on the parent Au/mica substrate and after the transfer onto a Si wafer with 300 nm SiO_2, respectively. On the Au substrate the typical Au(111) topography is observed with a root mean square roughness (RMS) of ≈0.5 nm. The effective thickness of Ru^{II} CNMs **2b**, estimated from the attenuation of the XPS Au $4f_{7/2}$ signal, is ≈0.6 nm. After the transfer, an apparent step edge height of ≈1.4 nm is determined by AFM between the nanosheet and the SiO_2 substrate (Figure 2b). The RMS value of the CNM area is ≈0.9 nm compared to an RMS value of ≈0.2 nm for the Si wafer. The

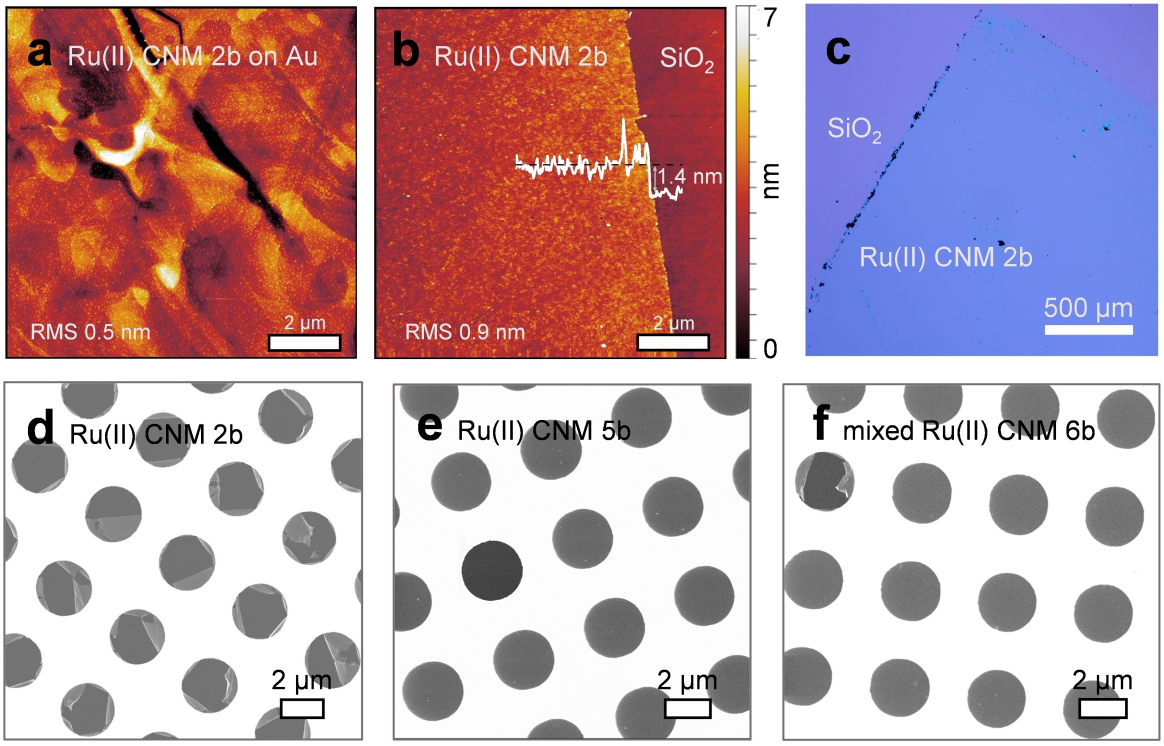

Figure 2. Atomic force microscopy images of Ru^{II} CNM **2b** a) on Au and b) after transfer to SiO_2/Si wafers. In (b) the line profile of the nanosheets edge on SiO_2 is shown in white. c) Optical micrograph of nanosheet **2b** on Si wafer. d)–f) Scanning electron micrographs of different Ru^{II} CNMs transferred to Quantifoil TEM grids. In (d) Ru^{II} CNM **2b** shows ruptures. Variation of self-assembly conditions for e) CNM **5b** and f) CNM **6b** leads to large free-standing areas.

optical micrograph[14] in Figure 2c verifies the formation of a large area and continuous nanosheet. Figure 2d displays an SEM image of the nanosheet on a transmission electron microscope (TEM) grid (see also Figure S1). It can be clearly recognized that Ru^{II} CNM **2b** forms free-standing areas although many ruptures are present. To improve the mechanical stability, we change the self-assembly conditions to increase the thickness of the initial SAM either by rising the self-assembly temperature to 50 °C (Ru^{II} SAM **5a**) or by using mixed SAMs with NBPT **3** (mixed Ru^{II} SAM **6a**).[10] According to the XPS analysis, the thickness of the formed nanosheets (Ru^{II} CNM **5b** and Ru^{II} CNM **6b**) on Au corresponds to ≈1.2 nm (see Scheme 1). Figures 2e,f present SEM images of the Ru^{II} CNMs **5b** and **6b** (see also Figures S2 and S3). Both the increased temperature and the mixed SAMs lead to molecular nanosheets with largely intact, free-standing areas.

Next, we characterize changes of the Ru^{II} complexes upon cross-linking using XPS. Figure 3a shows the high-resolution XP spectra of a Ru^{II} SAM **2a** before and after cross-linking to Ru^{II} CNM **2b** on Au as well as after transfer on a SiO_2/Si wafer. A detailed peak analysis can be found in the Supporting Information Table S1. The C 1s spectrum of Ru^{II} SAM **2a** reveals different peaks with the main components C_1 at a binding energy (BE) of 284.6 eV corresponding to aromatic and aliphatic carbon (full width at half maximum (FWHM) 1.2 eV) and C_2 carbon bound to nitrogen (BE = 285.6 eV, FWHM = 1.2 eV) alongside with a Ru $3d_{5/2}$ peak at a BE of 280.7 eV (FWHM = 1.4 eV).[10] The bipyridine nitrogen atoms result in a N 1s peak at 399.8 eV (FWHM = 1.5 eV). The O 1s binding energy region reveals two peaks: Carboxylates oriented towards the substrate[10,15] (530.8 eV, FWHM = 2.1 eV) and adsorbed oxygen R-OH species (532.5 eV, FWHM = 2.1 eV). The PF_6^- counterions are found in the SAM in an substoichiometric amount of $Ru:PF_6^- = 1:0.13$, as indicated in the F 1s XP spectrum by a small peak at 686.4 eV (FWHM = 1.9 eV, Figure S4). The reduced number of counterions presumably results from the deprotonation of the carboxylic acid groups upon self-assembly.[10] The thickness of Ru^{II} SAM **2a** is ≈0.9 nm. These characteristics of Ru^{II} SAM **2a** correspond very well to the results of Ref. [10] where the self-assembly of complex **1** on gold was studied at various experimental conditions in detail. The low-energy electron beam irradiation induced cross-linking to Ru^{II} CNM **2b** leads to several changes in the XP spectra. First, the effective thickness of the nanosheet reduces to 0.6 nm, which is similar to earlier reports on the cross-linking of various aromatic SAMs.[9b] For the C 1s main component C_1 at 284.7 eV, the FWHM broadens from 1.2 to 1.5 eV and the component area reduces by ≈26 %. FWHM of C_2 increases as well to 1.5 eV. The N 1s and Ru $3d_{5/2}$ peak positions remain similar, their FWHM broaden to 1.9 and 1.7 eV, respectively. However, the overall peak areas of N 1s and Ru $3d_{5/2}$ components decrease only by ≈6 %. The O 1s components BE positions remain similar, but the intensities of both peaks reduce

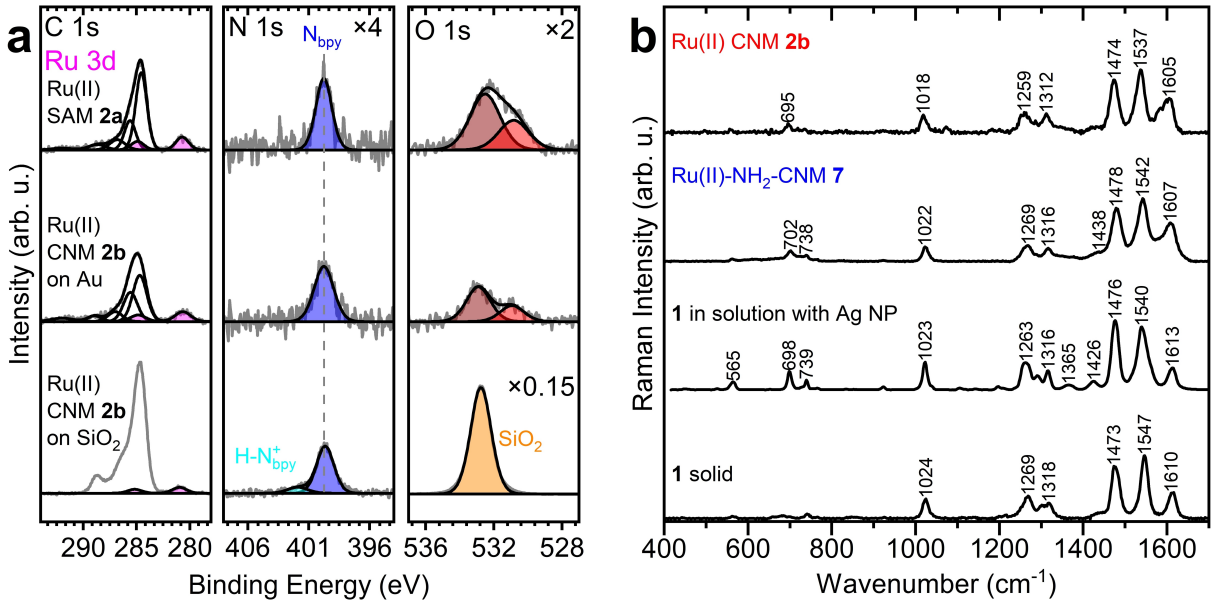

Figure 3. Changes in the molecular structure of the Ru^{II} polypyridine complex during cross-linking. a) XP spectra of the Ru^{II} complex SAM **2a** and CNM **2b** on gold surface and CNM **2b** on SiO_2/Si. In the bottom row, spectra of the transferred nanosheet show additional species assigned to protonated bipyridine (light blue) and SiO_2 (orange). N 1s and O 1s spectra are magnified by the indicated factors for better visualization. b) Raman spectra of Ru^{II} CNM **2b**, the hierarchical nanosheet Ru^{II}-NH_2-CNM **7** as well as Ru^{II} complex **1** in solution with Ag nanoparticles and as solid.

significantly by ≈50 % and their FWHM decrease to 1.7 eV. The PF_6^- counterions cannot be detected anymore. We interpret these changes as C–H bond cleavage,[11] partial desorption of methyl[16] and carboxylate groups,[17] and C–C bond formation on the bipyridine ligands indicated by the broadening of N 1s, Ru $3d_{5/2}$ and C 1s components, similar as reported for other aromatic SAMs.[18] The reduced peak areas suggest the desorption of only very few metal ions and nitrogen atoms during the electron irradiation in ultra-high vacuum. The main material loss occurs for the oxygen species, aromatic or aliphatic carbon groups and PF_6^- counterions.

Figure 3a (bottom row) shows the XP spectra for the Ru^{II} CNM **2b** transferred from the parent Au substrate to a SiO_2/Si wafer. Similar as for Ru^{II} CNM **2b**, the characteristic Ru $3d_{5/2}$ and N 1s bipyridine species of the complex are observed also after the transfer. The only differences are the presence of additional C 1s components due to poly(methyl methacrylate) (PMMA)[19] residues as well as appearance of a small amount of protonated pyridine species[20] (BE = 401.9 eV, FWHM = 2.0 eV). Noteworthy, the elemental ratio of Ru:N is reduced from ≈1:6.2 for Ru^{II} CNM **2b** on gold to ≈1:8.7 on SiO_2. The loss of some Ru^{II} ions during the transfer procedure may result from their insufficient coordination after the cross-linking. The XPS results for Ru^{II} SAMs and CNMs **5** and **6** are summarized in Figure S5, S6 and Table S1. These thicker samples show similar spectroscopic features and characteristic changes upon the cross-linking as observed for samples **2a**,**b**. For the mixed monolayer **6a**, the presence of NBPT is reflected by additional N 1s and S $2p_{3/2}$ signals of the nitro and thiolate groups, respectively.

Ru^{II}-NH_2-CNM **7** was prepared and analyzed in order to compare the photosensitizer nanosheets **2b**, **5b** and **6b** synthesized directly via electron irradiation of SAMs with a hierarchically assembled 2D reference system obtained via conventional grafting. To this end, NH_2-CNM **4b** with terminal amino groups was functionalized with Ru^{II} complex **1** via amidation (Scheme 1). The XPS data for the Ru^{II} complex in **7** reveal similar features as obtained for the Ru^{II} CNMs (Figure S7, Table S1). These similarities indicate the preservation of the Ru^{II} complex functionality after the electron irradiation induced cross-linking. To prove this assumption, we conducted a comparative study of Ru^{II} CNMs and Ru^{II}-NH_2-CNM by Raman and absorption spectroscopy which is presented below.

Using surface-enhanced resonance Raman scattering (SERRS) upon excitation at 476 nm with Ag nanoparticles drop-casted on the CNMs surfaces (Figure 3b, S8), it was possible to record resonance enhanced Raman spectra from both Ru^{II} CNM **2b** and Ru^{II}-NH_2-CNM **7** (see Figure 4a,b for the UV/Vis spectrum of **1** in $CHCl_3$). Figure 3b summarizes the Raman spectra of Ru^{II} CNM **2b**, Ru^{II}-NH_2-CNM **7** and Ru^{II} complex **1** in solution with silver nanoparticles. Raman spectra of a powder sample of complex **1** are depicted for comparison. The spectra of Ru^{II}-NH_2-CNM **7**, Ru^{II} CNM **2b** and solid reference are very similar both in band position and intensity ratios. In agreement with literature, they show three strong vibrations at ≈1474, 1537 and 1605 cm^{-1} and weaker bands at 1259, 1312, 1018 and 695 cm^{-1}.[21] These band positions are also observed for complex **1** in solution with Ag nanoparticles. Nonetheless, the intensity pattern differs. According to Ref. [21a] these differences are caused by the adsorption of the carboxylated

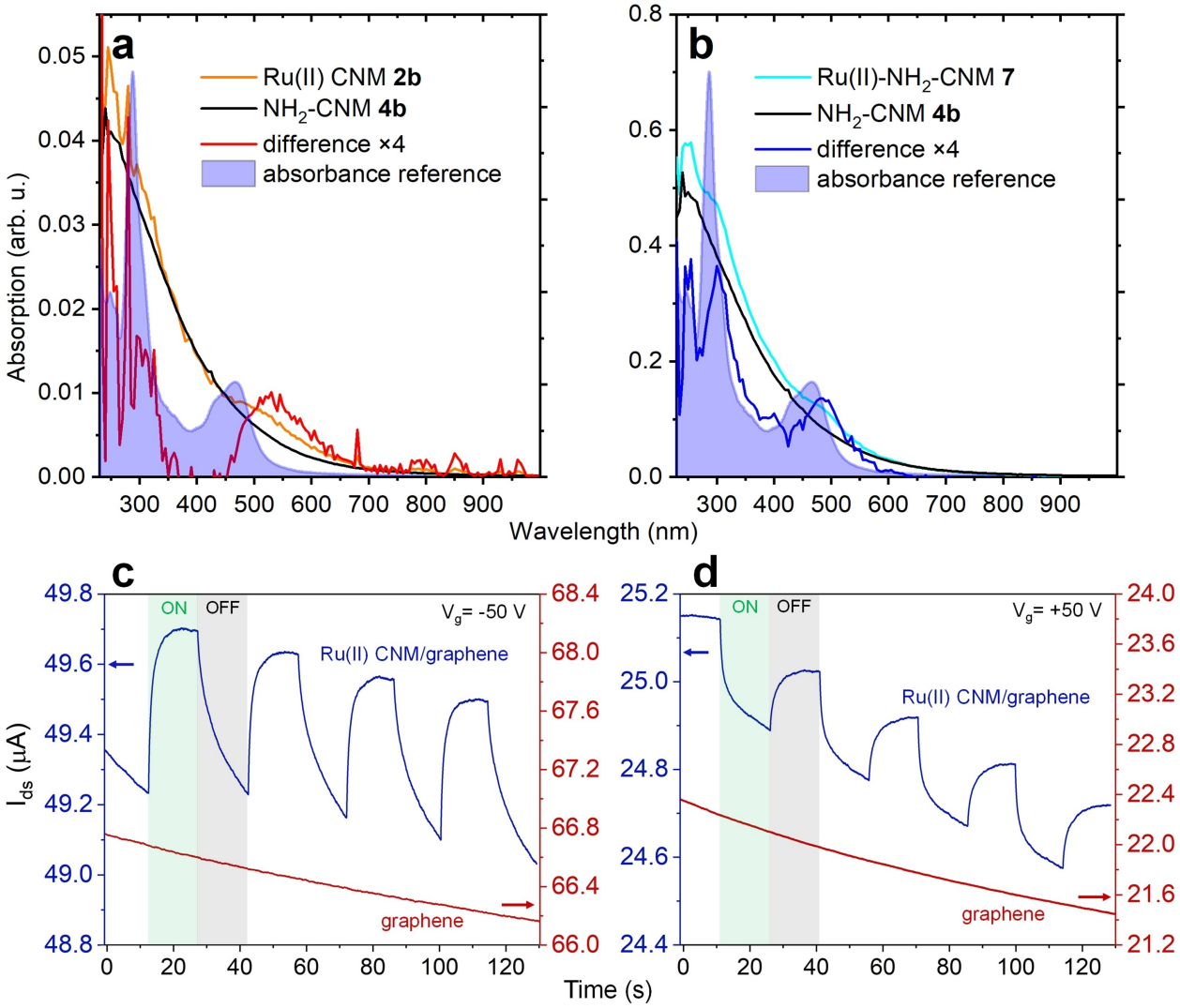

Figure 4. Absorption spectra obtained by photothermal deflection spectroscopy of a) Ru^{II} CNM **2b** (orange) and b) Ru^{II}-NH_2-CNM **7** (light blue) using as fluorinated solvent 3 M™ Fluorinert™ FC-770. The difference spectra of Ru^{II} CNM **2b** (red) and Ru^{II}-NH_2-CNM **7** (dark blue) with NH_2-CNM **4b** (black) resemble the characteristic features of the reference absorption spectra of complex **1** in $CHCl_3$ solution (purple). The photocurrent response I_{ds} of a Ru^{II} CNM/GFET device (blue-colored) upon ON/OFF switching of a 520 nm laser (80 μW cm^{-2}, V_{ds} = 0.1 V) is shown at c) V_g = −50 V and d) V_g = +50 V. The Ru^{II} CNM thickness is ≈3 nm. The current responses I_{ds} of a bare GFET reference device under the same laser switching are displayed in red in the dual y-axis graphs.

bipyridine ligand of the Ru^{II} complex on the Ag nanoparticle surface leading to a different enhancement mechanism as well as an overall higher Raman signal. The similarity between the Raman signatures of Ru^{II} CNM **2b**, Ru^{II}-NH_2-CNM **7** and solid reference **1** suggests that a substantial fraction of complexes preserve their vibrational and therewith physicochemical features after the electron irradiation induced cross-linking into a CNM, which is tested next by measuring their absorption spectra.

The absorption characteristics of a photosensitizer membrane are key for their applications in photocatalysis. Hence, we utilize photothermal deflection spectroscopy (PDS)[22] to probe the absorption of the Ru^{II} CNMs as chromophores. Figure 4a compares the absorption spectra of Ru^{II} CNM **2b** (orange, Figure 4a) to the spectrum of a bare NH_2-CNM **4b** (black). The latter serves as reference spectrum and was recorded from a stack of eight layers to increase the inherently low signal to noise ratio of individual only ≈1 nm thick nanosheets. Calculating the spectral differences between the absorption of both nanosheets (red), reveals characteristic metal-to-ligand charge transfer (MLCT) absorption features at ≈530 nm, similar as reported for the SAMs of Ru^{II} polypyridine compounds on glass[23] or ITO.[24] Compared to the spectrum of **1** in $CHCl_3$ solution the absorption band of Ru^{II} CNM **2b** is broader and shifted to longer wavelengths. PD spectra were also taken for the hierarchical Ru^{II}-NH_2-CNM **7** with covalently attached complexes. Also, here a stack of eight layers of **7** was probed to increase the signal to noise ratio and the difference spectrum (relative to bare NH_2-CNM **4b**) shows absorption

characteristics of the parent Ru^{II} complex. The observed red shift of the MLCT absorption originates most likely from some alteration of the chromophore properties in these 2D assemblies.[25] A minor contribution can also result from different solvents used for the PDS measurements and for measurements of the reference **1** (see caption to Figure 4 and Supporting Information for details).[25b,26]

To further demonstrate the photo-activity of the Ru^{II} CNMs, we assembled their van der Waals heterostructures with graphene[27] and studied the photo-response of the respective field-effect transistors (GFET) upon irradiation at 520 nm (see Figure S10). Within the same chip, both Ru^{II} CNM/GFET devices and bare GFETs were characterized, which enabled the use of the latter as reference (see Figure S10c). Figures 4c and 4d show the photo-response of both types of devices upon periodic irradiation at the gate voltages, V_g, of -50 V and $+50$ V, respectively. The Ru^{II} CNM/graphene devices display a photo-current upon irradiation; whereas, the bare graphene devices do not show any photo-response. We attribute the observed behavior to the reduction of Ru^{3+} centers, which were generated upon the light absorption, to Ru^{2+} via electron transfer from graphene. The GFET transport curves of a Ru^{II} CNM/GFET under dark conditions and under illumination (see Figure S11a, b) clearly show an up-shifting of the graphene Dirac point voltage (V_D) by increasing the laser intensity, which demonstrates an increase of the *p*-type doping[28] (see Figure S11c,d). Such a behavior results in an increase/decrease of the photocurrent at $V_g = -50$ V (i.e., $V_g < V_D$) and at $V_g = +50$ V (i.e., $V_g > V_D$), respectively (cf. Figures 4c, d). Notably, in Figures 4c,d a Ru^{II} CNM with a nominal thickness of ≈ 3 nm was used. A similar photo-response was also observed for the monolayer Ru^{II} CNM 2b/GFET devices, Figure S12. However, as the amount of photo-active material in these devices is very low, a higher laser power needs to be applied, which results in overlapping of their genuine photo-response with the photo-gating of the underlying SiO_2.

In summary, we have demonstrated that low-energy electron irradiation of Ru^{II} complex SAMs enables their conversion into large area ≈ 1 nm thick molecular photosensitizer nanosheets. A comparison of the spectroscopic characteristics of these nanosheets with the parent Ru^{II} complexes and the hierarchically assembled nanosheets shows the preservation of the functional photoactive properties. Therewith, we suggest an alternative route to engineer 2D molecular free-standing systems for applications in photocatalysis and photoinduced energy conversion.

Acknowledgements

The authors thank Nicole Fritz (ESI MS) and Sandra Köhn (elemental analysis). Furthermore, we acknowledge experimental assistance by Lara S. Dröge during the initial stages of the experiments. This work was supported financially by the Deutsche Forschungsgemeinschaft (DFG) within the CRC-TRR 234 "CataLight" projects B01, B02, B07, C01, C04 and Z02. A.W. and U.S.S. acknowledge funding by the DFG within the priority program 2102 "LCRMC" under the grant number SCHU1229-16/1. Furthermore, M.K. and A.T. thank the DFG for financial support within the research grant TU149/8-2 and infrastructure grant INST 275/357-1 FUGG. Open Access funding enabled and organized by Projekt DEAL.

Conflict of Interest

The authors declare no conflict of interest.

Data Availability Statement

The data that support the findings of this study are available from the corresponding author upon reasonable request.

Keywords: 2D Materials · Monolayers · Nanomembranes · Nanostructures · Ruthenium Sensitizers · Surface Chemistry

[1] a) Z. Abdin, A. Zafaranloo, A. Rafiee, W. Mérida, W. Lipiński, K. R. Khalilpour, *Renewable Sustainable Energy Rev.* **2020**, *120*, 109620; b) M. D. Kärkäs, O. Verho, E. V. Johnston, B. Åkermark, *Chem. Rev.* **2014**, *114*, 11863–12001.
[2] T. P. Yoon, M. A. Ischay, J. Du, *Nat. Chem.* **2010**, *2*, 527–532.
[3] B. Zhang, L. Sun, *Chem. Soc. Rev.* **2019**, *48*, 2216–2264.
[4] X. Liu, S. Inagaki, J. Gong, *Angew. Chem. Int. Ed.* **2016**, *55*, 14924–14950; *Angew. Chem.* **2016**, *128*, 15146–15174.
[5] a) T. Su, Q. Shao, Z. Qin, Z. Guo, Z. Wu, *ACS Catal.* **2018**, *8*, 2253–2276; b) J. Di, J. Xiong, H. Li, Z. Liu, *Adv. Mater.* **2018**, *30*, 1704548; c) D. Deng, K. S. Novoselov, Q. Fu, N. Zheng, Z. Tian, X. Bao, *Nat. Nanotechnol.* **2016**, *11*, 218–230; d) C. Backes, et al., *2D Mater.* **2020**, *7*, 022001.
[6] a) X. Zhang, C. Neumann, P. Angelova, A. Beyer, A. Gölzhäuser, *Langmuir* **2014**, *30*, 8221–8227; b) Y. Yang, P. Dementyev, N. Biere, D. Emmrich, P. Stohmann, R. Korzetz, X. Zhang, A. Beyer, S. Koch, D. Anselmetti, A. Gölzhäuser, *ACS Nano* **2018**, *12*, 4695–4701; c) E. Griffin, L. Mogg, G. P. Hao, G. Kalon, C. Bacaksiz, G. Lopez-Polin, T. Y. Zhou, V. Guarochico, J. Cai, C. Neumann, A. Winter, M. Mohn, J. H. Lee, J. Lin, U. Kaiser, I. V. Grigorieva, K. Suenaga, B. Özyilmaz, H. M. Cheng, W. Ren, A. Turchanin, F. M. Peeters, A. K. Geim, M. Lozada-Hidalgo, *ACS Nano* **2020**, *14*, 7280–7286; d) K. G. Zhou, K. S. Vasu, C. T. Cherian, M. Neek-Amal, J. C. Zhang, H. Ghorbanfekr-Kalashami, K. Huang, O. P. Marshall, V. G. Kravets, J. Abraham, Y. Su, A. N. Grigorenko, A. Pratt, A. K. Geim, F. M. Peeters, K. S. Novoselov, R. R. Nair, *Nature* **2018**, *559*, 236–240.
[7] Z. Zheng, C. T. Nottbohm, A. Turchanin, H. Muzik, A. Beyer, M. Heilemann, M. Sauer, A. Gölzhäuser, *Angew. Chem. Int. Ed.* **2010**, *49*, 8493–8497; *Angew. Chem.* **2010**, *122*, 8671–8675.
[8] a) U. Schmelmer, R. Jordan, W. Geyer, W. Eck, A. Gölzhäuser, M. Grunze, A. Ulman, *Angew. Chem. Int. Ed.* **2003**, *42*, 559–563; *Angew. Chem.* **2003**, *115*, 577–581; b) J. Scherr, Z. Tang, M. Küllmer, S. Balser, A. S. Scholz, A. Winter, K. Parey, A. Rittner, M. Grininger, V. Zickermann, D. Rhinow, A. Terfort, A. Turchanin, *ACS Nano* **2020**, *14*, 9972–9978.
[9] a) A. Turchanin, A. Gölzhäuser, *Adv. Mater.* **2016**, *28*, 6075–6103; b) P. Angelova, H. Vieker, N.-E. Weber, D. Matei, O. Reimer, I. Meier, S. Kurasch, J. Biskupek, D. Lorbach, K. Wunderlich, L. Chen, A. Terfort, M. Klapper, K. Müllen, U.

Kaiser, A. Gölzhäuser, A. Turchanin, *ACS Nano* **2013**, *7*, 6489–6497.
[10] M. Küllmer, P. Endres, S. Götz, A. Winter, U. S. Schubert, A. Turchanin, *ACS Appl. Mater. Interfaces* **2021**, *13*, 60544–60552.
[11] C. Neumann, R. A. Wilhelm, M. Küllmer, A. Turchanin, *Faraday Discuss.* **2021**, *227*, 61–79.
[12] A. Turchanin, D. Käfer, M. El-Desawy, C. Wöll, G. Witte, A. Gölzhäuser, *Langmuir* **2009**, *25*, 7342–7352.
[13] Z. Tang, C. Neumann, A. Winter, A. Turchanin, *Nanoscale* **2020**, *12*, 8656–8663.
[14] C. T. Nottbohm, A. Turchanin, A. Beyer, R. Stosch, A. Gölzhäuser, *Small* **2011**, *7*, 874–883.
[15] H. Aitchison, H. Lu, S. W. Hogan, H. Früchtl, I. Cebula, M. Zharnikov, M. Buck, *Langmuir* **2016**, *32*, 9397–9409.
[16] M. Zharnikov, W. Geyer, A. Gölzhäuser, S. Frey, M. Grunze, *Phys. Chem. Chem. Phys.* **1999**, *1*, 3163–3171.
[17] C. Neumann, M. Szwed, M. Frey, Z. Tang, K. Koziel, P. Cyganik, A. Turchanin, *ACS Appl. Mater. Interfaces* **2019**, *11*, 31176–31181.
[18] a) W. Eck, V. Stadler, W. Geyer, M. Zharnikov, A. Gölzhäuser, M. Grunze, *Adv. Mater.* **2000**, *12*, 805–808; b) C. Yildirim, E. Sauter, A. Terfort, M. Zharnikov, *J. Phys. Chem. C* **2017**, *121*, 9982–9990.
[19] A. P. Pijpers, R. J. Meier, *Chem. Soc. Rev.* **1999**, *28*, 233–238.
[20] F. Schiffmann, J. VandeVondele, J. Hutter, R. Wirz, A. Urakawa, A. Baiker, *J. Phys. Chem. C* **2010**, *114*, 8398–8404.
[21] a) M. Kokošková, M. Procházka, I. Šloufová, B. Vlčková, *J. Phys. Chem. C* **2013**, *117*, 1044–1052; b) M. J. Edmiston, R. D. Peacock, *Spectrochim. Acta Part A* **1993**, *49*, 1481–1486; c) P. A. Mabrouk, M. S. Wrighton, *Inorg. Chem.* **1986**, *25*, 526–531.
[22] a) M. L. Hupfer, F. Herrmann-Westendorf, B. Dietzek, M. Presselt, *Analyst* **2021**, *146*, 5033–5036; b) M. L. Hupfer, F. Herrmann-Westendorf, M. Kaufmann, D. Weiß, R. Beckert, B. Dietzek, M. Presselt, *Chem. Eur. J.* **2019**, *25*, 8630–8634; c) W. B. Jackson, N. M. Amer, A. C. Boccara, D. Fournier, *Appl. Opt.* **1981**, *20*, 1333–1344.
[23] P. C. Mondal, V. Singh, Y. L. Jeyachandran, M. Zharnikov, *J. Phys. Chem. C* **2019**, *123*, 6121–6129.
[24] R. Balgley, Y. M. Algavi, N. Elool Dov, M. Lahav, M. E. van der Boom, *Angew. Chem. Int. Ed.* **2018**, *57*, 13459–13464; *Angew. Chem.* **2018**, *130*, 13647–13652.
[25] a) S. F. McClanahan, R. F. Dallinger, F. J. Holler, J. R. Kincaid, *J. Am. Chem. Soc.* **1985**, *107*, 4853–4860; b) M. Kovács, K. L. Ronayne, W. R. Browne, W. Henry, J. G. Vos, J. J. McGarvey, A. Horváth, *Photochem. Photobiol. Sci.* **2007**, *6*, 444–453.
[26] a) K. W. Lee, J. D. Slinker, A. A. Gorodetsky, S. Flores-Torres, H. D. Abruña, P. L. Houston, G. G. Malliaras, *Phys. Chem. Chem. Phys.* **2003**, *5*, 2706–2709; b) E. E. Beauvilliers, G. J. Meyer, *Inorg. Chem.* **2016**, *55*, 7517–7526.
[27] M. Woszczyna, A. Winter, M. Grothe, A. Willunat, S. Wundrack, R. Stosch, T. Weimann, F. Ahlers, A. Turchanin, *Adv. Mater.* **2014**, *26*, 4831–4837.
[28] S. Goniszewski, M. Adabi, O. Shaforost, S. M. Hanham, L. Hao, N. Klein, *Sci. Rep.* **2016**, *6*, 22858.

Manuscript received: April 5, 2022
Accepted manuscript online: April 13, 2022
Version of record online: May 9, 2022